Microstrip and Stripline Ferrite-Coupled-Line (FCL) Circulators

Cham Kiong Queck, *Student Member, IEEE*, and Lionel E. Davis, *Life Fellow, IEEE*

***Abstract*—Measurements on an 11-GHz four-port microstrip ferrite-coupled-line (FCL) circulator, employing a broad-band hybrid coupler and an improved air bridge, confirm that only a weak biasing field of 3–4 kA/m (35–50 Oe) is required. By cascading the S-matrices of the FCL section and hybrid coupler using signal flow graphs, the measured and predicted bandwidth and losses are compared for the first time. Simulated results for stripline FCL sections exhibit broader bandwidths than those obtained with microstrip FCL sections. Using such a structure, the simulated performance of a three-port circulator indicates that, in principle, bandwidths of at least 3 : 1 or 4 : 1 may be possible.**

***Index Terms*—Broad-band, coupled transmission lines, ferrite circulators, losses.**

I. Introduction

COMPARED TO A conventional junction circulator, a ferrite-coupled-line (FCL) circulator has the potential advantages of broad bandwidth and the need for only a small bias field, and the potential disadvantages of higher loss and greater size. The purpose of this paper is to begin to address some of these issues.

Since the experimental discovery [1] of the nonreciprocal behavior of longitudinally magnetized FCLs, several papers [2]–[7] have proposed methods of analysis and conditions for optimum operation. A proof-of-principle experiment [7] demonstrated the nonreciprocal behavior of a three- and four-port "microstrip" circulator with the ferrite above the substrate. However, multiple reflections were observed and the differential isolation was poor (approximately 6 dB). To improve the performance, three- and four-port stripline-type ferrite-on-top circulators with matching transformers at the ferrite/dielectric interfaces were designed and measured [8]. The previous multiple reflections were reduced, but reflections from the hybrid coupler became evident. In this paper, the measured and predicted performance of a four-port microstrip FCL circulator with a ferrite substrate and an improved coupler and air bridge is reported. The performance of the circulator with and without conductor loss is predicted by cascading the FCL section with the hybrid coupler using signal flow graphs. The separate bandwidth-limiting effects of the coupler and FCL are discussed and the need for a broader bandwidth FCL section is seen. Stripline FCLs have broader bandwidths than microstrip FCLs [6] and the simulated performance is presented for the first time of a three-port FCL circulator with an operating bandwidth of at least 10–40 GHz. The simulated performance of a four-port circulator consisting of two three-port devices is compared with the simulated performance of a "perfect" four-port circulator with a hybrid coupler. The effects of relative permittivity are also briefly considered.

Manuscript received April 5, 2002; revised August 15, 2002.

The authors are with The Electromagnetics Centre for Microwave and Millimeter-Wave Design and Applications, Department of Electrical Engineering and Electronics, University of Manchester Institute of Science and Technology, Manchester M60 1QD, U.K. (e-mail: mchpicq2@stud.umist.ac.uk; l.davis@umist.ac.uk).

Digital Object Identifier 10.1109/TMTT.2002.805184

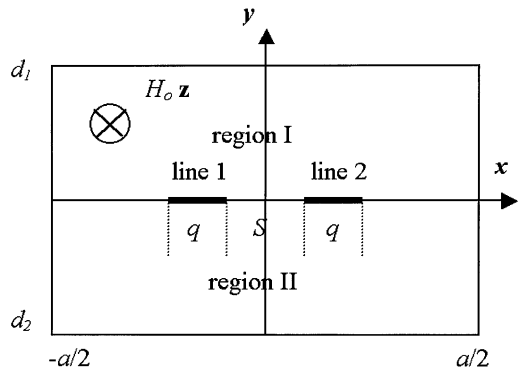

Fig. 1. Cross section of the FCL structure. Regions I or II can be a ferrite. $\boldsymbol{H_o} = H_o z$.

II. Theory

Three- or four-port FCL circulators can be realized by cascading the FCL sections with a T-junction or a hybrid coupler, respectively. Alternatively, a four-port circulator can be produced by cascading two three-port circulators. An FCL is a structure that has a pair of closely spaced parallel lines with magnetized ferrite loading. Fig. 1 shows the cross section of the FCL in which S is the separation between the two coupled lines of width q, and d_1, d_2 are the thickness of the superstrate (region I) and substrate (region II), respectively. Either regions I or II can be a ferrite. The metallic enclosure has a width a, which is typically set to a value $a = 6(2q + S)$, and for microstrip modeling, $d_1 = 10d_2$. The enclosure serves to suppress radiation losses, as well as being convenient for the finite-element method. A biasing magnetic field is applied longitudinally in the direction of propagation, i.e., perpendicular to the cross section. Using normal mode analysis, the condition for an equal power output is given by [4]

$$L = \frac{(1+2n)\,\pi}{2\,(\beta_1 - \beta_2)} \tag{1}$$

where L is the length of the FCL section, and β_1, β_2 are propagation constants for mode 1 (RHCP) and mode 2 (LHCP) of the magnetized FCL. To minimize the length, n is normally set

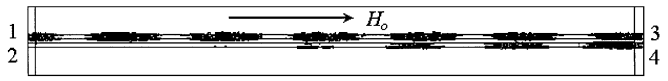

Fig. 2. Electric-field distributions in the microstrip FCL section for signal input at port 1.

to zero. The expected behavior of the FCL section satisfying (1) is described in [5] and [6] and will not be discussed here. It is shown in [2] that the strongest coupling effect occurs when $\beta_{\text{even}} = \beta_{\text{odd}}$ for an unmagnetized structure and, therefore, for microstrip or slotline FCLs, the optimal operating frequency can be defined [4] as the frequency at which the propagation constant curves for β_{even} and β_{odd} intersect. However, this definition cannot be used for TEM structures such as the stripline FCL for which $\beta_{\text{even}} = \beta_{\text{odd}}$ in the unmagnetized state. In [6], it was shown that, potentially, the stripline FCLs have broad bandwidths and a power transfer factor (PTF) and power isolation factor (PIF) was defined. These factors take into account reflections at the ferrite/dielectric interface at both ends of the FCL, and they enable the performance of different structures to be compared.

III. Four-Port Microstrip FCL Circulator

A four-port microstrip FCL circulator consisting of two components, i.e., a microstrip FCL section and a 180° hybrid coupler with an air bridge, was analyzed in terms of its separate components and the overall performance was predicted and measured.

A. Microstrip FCL Section

For convenience of fabrication, a microstrip FCL with a ferrite as a substrate was selected with the following parameters [6]: ferrite magnetization and relative permittivity $M_s = 239$ kA/m ($4\pi M_s = 3000$ G) and $\varepsilon_f = 12$, $d_2 = 0.2$ mm, $d_1 = 2$ mm, $q = 0.16$ mm, and $S = 0.2$ mm. Using (1) for an equal power output condition, $L = 36$ mm and this structure was simulated using Ansoft HFSS software. The simulated electric-field strength distribution along the FCL at 11.4 GHz is shown in Fig. 2 where coupling occurs and signals emerge from ports 3 and 4, when a signal is fed into port 1. As reported in [9], the predicted bandwidth for this structure is from 9.75 to 11.25 GHz, where the insertion loss is from -3.75 to -2.5 dB, and the isolation S_{21} and reflection loss S_{11} are below -14 dB. Note that the bandwidth in this paper is defined at a fixed length, whereas in [6], the bandwidth is defined using a variable optimum length. When a signal is fed into port 2 instead of port 1, an odd signal emerges from the output ports instead of an even signal. The phase characteristics of the microstrip FCL when the signal is fed into ports 1 or 2 are shown in Fig. 3 and we observe that even or odd output signals (respectively) occur at approximately 10.3 GHz, i.e., at a frequency 10% lower than predicted. Over the bandwidth, the maximum value for both $|\angle S_{31} - \angle S_{41}|$ and $|\angle S_{32} - \angle S_{42} - 180°|$ is 20°. If the direction of magnetization is reversed, the outputs are odd (even) for an input at port 1 (2), and this behavior has been discussed earlier [2]–[7].

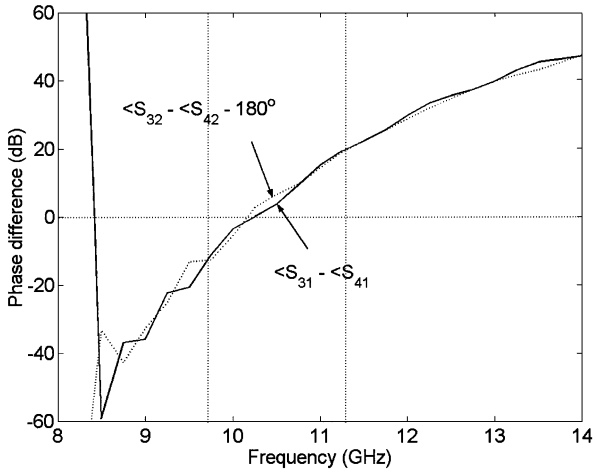

Fig. 3. Predicted frequency response of $\angle S_{31} - \angle S_{41}$ (solid line) and $\angle S_{32} - \angle S_{42} - 180°$ (dotted line) of the FCL section.

B. Broad-Band Hybrid Coupler With Improved Air Bridge

The step-impedance technique [10], [11] was used to design a broad-band rectangular hybrid coupler with an air bridge at 11.4 GHz on a substrate of relative permittivity $\varepsilon_r = 10.2$ and of thickness $h_a = 0.254$ mm. The optimized broad-band hybrid coupler is shown in Fig. 4, and the section impedances Z_1, Z_2, Z_3, Z_4, Z_{1C}, and Z_{2C} have values of 56.8, 46.6, 27.5, 16.7, 46.7, and 37.2 Ω, respectively, and each has an electrical length of 90° at the design frequency. The air bridge in the earlier four-port devices [7], [8] caused a degradation in performance due to reflection loss at the adjacent port. The reflection loss of an air bridge, however, can be minimized by introducing square pads of width S at both ends of the air bridge [12] using a design procedure described in [13]. Computation of an air bridge alone, without the coupler, using Momentum shows that the image impedance of an air bridge with a height of 0.25 mm, width of 0.4 mm, and length of 1.6 mm on a substrate of relative permittivity $\varepsilon_r = 10.2$ is reduced to 50 Ω when $S = 0.45$ mm. This results in the minimum reflection loss (-54 dB) occurring near 11.4 GHz, which is a significant improvement over the conventional design where the reflection loss is approximately -12 dB at 11.4 GHz. A wide bandwidth of 6 GHz (over 50% of the design frequency of 11 GHz) for the broad-band hybrid coupler with the improved air bridge has been reported in [9], and here we report the phase characteristics of that coupler. With reference to the port numbering in Fig. 4, the predicted values for both $\angle S_{43} - \angle S_{13}$ and $\angle S_{42} - \angle S_{12} - 180°$ at the band edges are approximately 25° and are zero at approximately 10.7 GHz, as can be seen in Fig. 5. The rectangular hybrid coupler design is preferred to the ring design as the former is neater, especially with the air bridge, and simulation shows that it has a slightly broader bandwidth than that of the latter.

C. Predicted Cascaded Performance

The cascaded design, in which the two isotropic sections (A and C) are matched to the ferrite section (region B) via quarter-wave transformers at 11.4 GHz, is shown in Fig. 6. By cascading the S-matrices of the FCL section and the hybrid

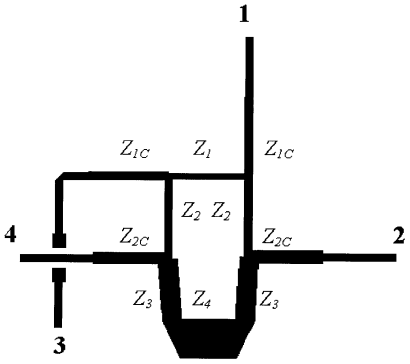

Fig. 4. Broad-band hybrid coupler with improved air-bridge design.

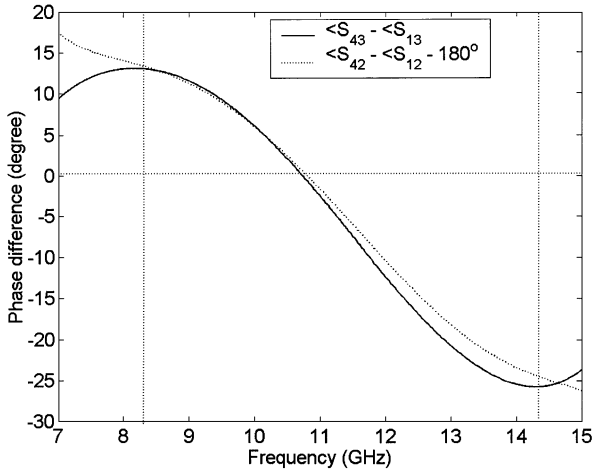

Fig. 5. Simulated frequency response of $\angle S_{43} - \angle S_{13}$ (solid line) and $\angle S_{42} - \angle S_{12} - 180^\circ$ (dotted line) of the hybrid coupler.

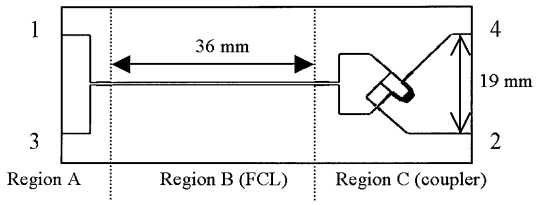

Fig. 6. Actual circuit of four-port microstrip FCL circulator (not actual size).

coupler, using signal flow graphs [14], the overall cascaded performance of the lossless structure (B and C) has been computed and are shown in Fig. 7. Region A was omitted for simplicity. Defining the bandwidth as the frequency range where insertion loss is less than 0.5 dB, we observe that the bandwidth is from 9.6 to 11.4 GHz and, over this bandwidth, the isolation (S_{12} and S_{31}) and reflection loss (S_{11}) are below -15 dB. It was also found that the predicted insertion loss curves for S_{32}, S_{43}, and S_{14} were similar to that of S_{21}, while the isolation curves S_{23}, S_{34}, and S_{41} were also below -15 dB. This predicted result clearly demonstrates the nonreciprocal behavior and circulation effect of the cascaded design.

D. Measurement of the Circulator

The fabricated FCL circulator circuits with gold tracks were mounted onto an aluminum jig, as shown in Fig. 8, and measured using an HP 8510C Network Analyzer. A rectangular uni-

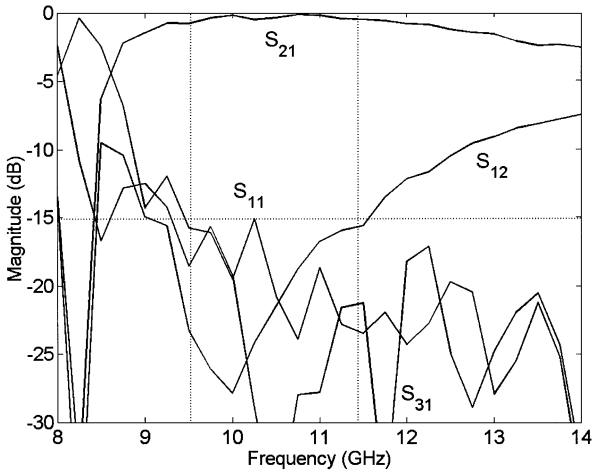

Fig. 7. Predicted frequency response of the four-port microstrip FCL circulator. Note that the air bridge is adjacent to port 2.

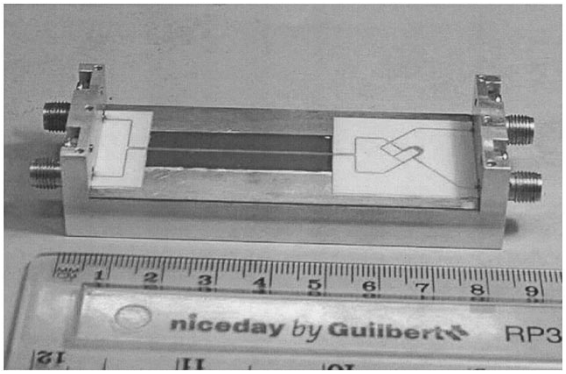

Fig. 8. Photograph of the four-port microstrip circulator in the aluminum jig.

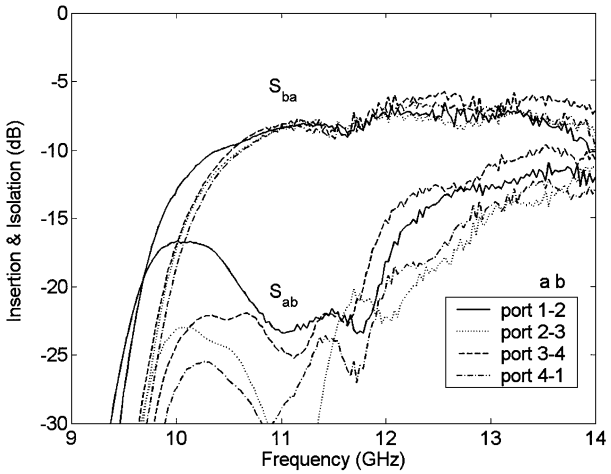

Fig. 9. Measured insertion loss and isolation at all ports.

form-field solenoid of cross section of 66 mm $\times$ 36 mm and of length of 132 mm was used to provide a static magnetic bias field. Fig. 9 shows the insertion loss and isolation between ports of the following combinations: 1–2, 2–3, 3–4, and 4–1, and it clearly shows that the direction of circulation is $1 \rightarrow 2 \rightarrow 3 \rightarrow 4 \rightarrow 1$. The measurement shows the improvements in this device compared to earlier devices, e.g., a more clearly defined region of nonreciprocity, and (as shown in Fig. 10) low reflec-

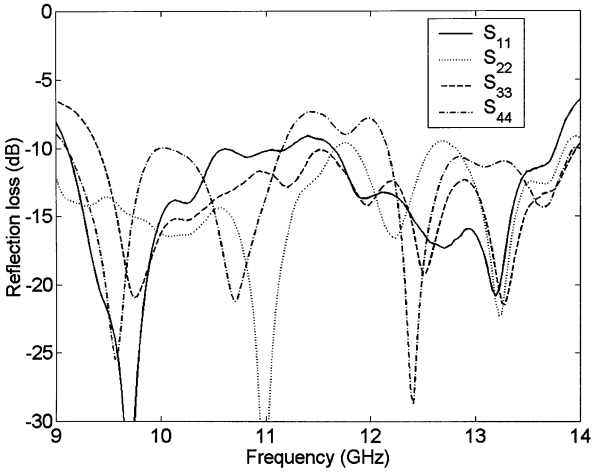

Fig. 10. Measured reflection loss measured at all ports.

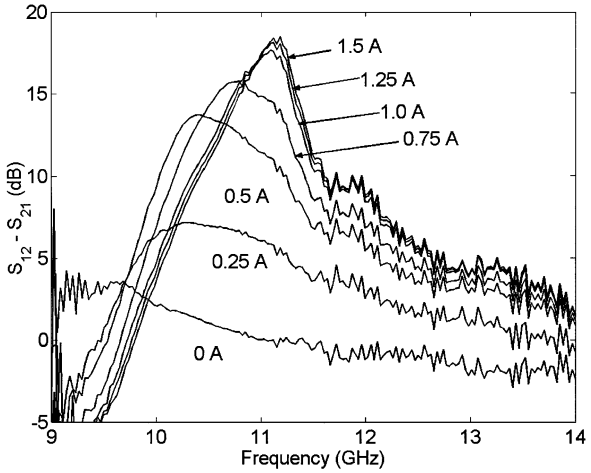

Fig. 11. Effect of magnetization current I_m to nonreciprocal behavior $|S_{12}| - |S_{21}|$ for $I_m = 0$ to 1.5 A at a step of 0.25 A. ($H_o = 0$–4 kA/m).

tion loss at port 2, which is located near to the improved air bridge. At 11 GHz, the insertion losses of S_{21}, S_{32}, S_{43}, and S_{14} are approximately -8 dB, and losses are discussed in Section III-E. The effect of bias field strength on the differential isolation $|S_{12}| - |S_{21}|$ is shown in Fig. 11, where the value of $|S_{12}| - |S_{21}|$ reaches a maximum near 11 GHz. As the magnetization current in the solenoid was increased to 1.0 A (equivalent to an applied static field of 2.8 kA/m) in steps of 0.25 A, $|S_{12}| - |S_{21}|$ increased to approximately 17 dB. Further increments up to 1.5 A (4.1 kA/m) produced little change in the nonreciprocity curve, hence, confirming the early theory that only a weak longitudinal bias field is needed for FCL circulators.

E. Losses in the Microstrip Circulator

Simulation using HFSS [9] shows that the predicted conductor loss in the four-port microstrip circulator (regions B and C only) is approximately 2 dB (within the bandwidth), assuming zero metal thickness and the conductivity of copper $\sigma = 5.8 \times 10^7$ S/m. To provide a simple comparison with the loss predicted by simulation, an alternative calculation was made assuming the signal was transmitted along sections of microstrip of different width between ports 1 and 2. This estimate was obtained using the formulas from Pucel *et al.* [15], who used Wheeler's microstrip equations [16] to derive the expression for conductor loss per unit length α_C (in decibels/unit length)

$$\alpha_C = \frac{R_S A_C}{Z_L h} \tag{2}$$

where R_s is the surface resistance, Z_L is the characteristic impedance of the microstrip, h is the dielectric thickness, and A_c (in decibels) is the geometry factor.

For $1/(2\pi) \le w/h \le 2$

$$A_C = \frac{8.68}{2\pi}\left\{1 - \left(\frac{w_{\rm eq}}{4h}\right)^2\right\} \cdot \left[1 + \frac{h}{w_{\rm eq}} + \frac{h}{\pi w_{\rm eq}}\left\{\ln\left(\frac{2h}{t}\right) - \frac{t}{h}\right\}\right] \tag{3a}$$

for $w/h > 2$

$$A_C = 8.68\left[\frac{w_{\rm eq}}{h} + \frac{\frac{w_{\rm eq}}{\pi h}}{\frac{w_{\rm eq}}{2h} + 0.94}\right] \cdot \left(\frac{\left[1 + \frac{h}{w_{\rm eq}} + \frac{h}{\pi w_{\rm eq}}\left\{\ln\left(\frac{2h}{t}\right) - \frac{t}{h}\right\}\right]}{\left[\frac{w_{\rm eq}}{h} + \frac{2}{\pi}\ln\left\{5.44\pi\left(\frac{w_{\rm eq}}{2h} + 0.94\right)\right\}\right]^2}\right). \tag{3b}$$

$w_{\rm eq}$ is the equivalent width for a microstrip with physical width w and metal thickness t, and the relationship is given by $w_{\rm eq} = w + \Delta w$, where Δw (for $w/h > 1/2\pi$) is the Wheeler's corrective term [16] in order to take the thickness of the metal strip into consideration, which is as follows:

$$\Delta w = \frac{t}{\pi}\left[\ln\left(\frac{2h}{t}\right) + 1\right]. \tag{4}$$

The term Δw is often negligible, except for very narrow strip width $w/h \ll 1$. For $t = 4$ μm, conductivity of gold $\sigma = 4.1 \times 10^7$ S/m and simply assuming that the signal follows only one path from ports 1 to 2 (in Fig. 9), the conductor loss for S_{21} is approximately 1.5 dB. This estimated loss may be slightly undervalued due to surface roughness (Δ), but assuming $\Delta = 80$ nm, the correction makes a negligible difference.

The dielectric loss (in decibels/unit length) of a microstrip is given by [17]

$$\alpha_D = 27.3\frac{\varepsilon_r\left(\varepsilon_{\rm eff} - 1\right)\tan\delta}{\sqrt{\varepsilon_{\rm eff}}\left(\varepsilon_r - 1\right)\lambda_g} \tag{5}$$

where ε_r and $\varepsilon_{\rm eff}$ are the dielectric constant and effective dielectric constant of the substrate, respectively, $\tan\delta$ is the loss tangent, and λ_g is the wavelength. Again, assuming a single path from ports 1 to 2, the calculated dielectric loss for S_{21} is 0.46 dB. Thus, the simulation and simple estimates suggest that both conductor and dielectric losses together may account for 2–3 dB at most. The extent to which other loss mechanisms such as magnetic loss and radiation and surface-wave loss contribute to the overall losses of the four-port circulator is not known at this stage.

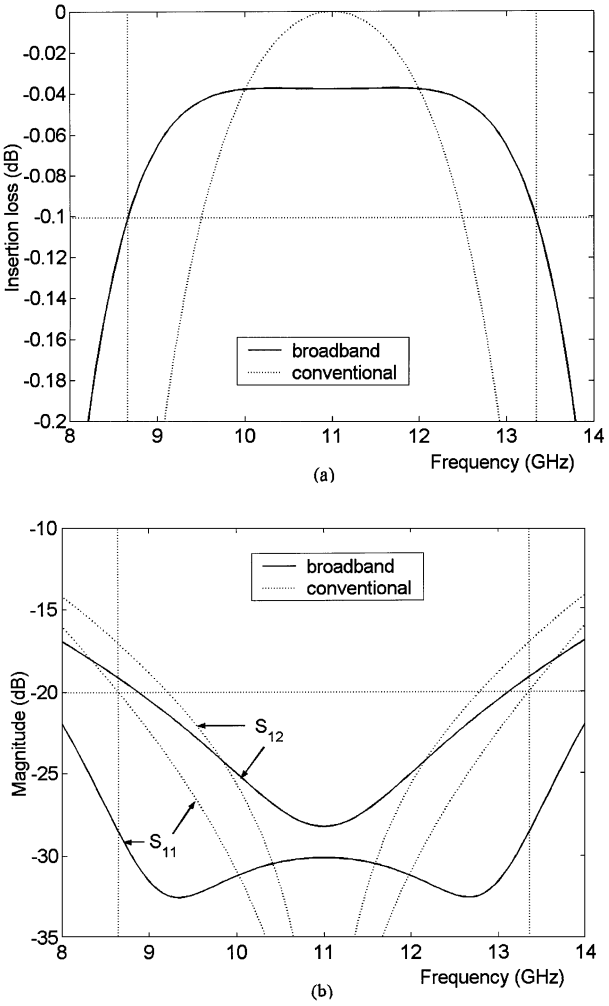

Fig. 12. Ideal performance of the broad-band and conventional four-port circulator in terms of: (a) insertion loss S_{21}, (b) isolation S_{12}, and reflection loss S_{11}.

IV. Broad-Band Four-Port FCL Circulator

The bandwidth of the circulator in Section III was limited by the bandwidth of the microstrip FCL section. The bandwidth could be broadened by the following.

- Replacing the microstrip FCL with a stripline FCL. Early investigation [6] revealed that stripline FCLs are potentially broad-band, which will be discussed in Section V
- Increasing the separation between the two coupled lines, which would reduce the coupling coefficient. However, this would be at the expense of a longer structure and would result in higher conductor loss.

To investigate the bandwidth limitation due to the broad-band coupler, a perfect FCL section was assumed, i.e., -3-dB outputs and zero phase difference over a specified frequency range, and cascaded it with an ideal broad-band hybrid coupler, which was analyzed using an even–odd method [11]. Using signal flow graphs, the predicted performances of the "perfect FCL" cascaded with an ideal coupler for both conventional and broad-band couplers were obtained and are shown in Fig. 12. The bandwidth (for insertion loss above -0.1 dB) with the broad-band hybrid is 4.7 GHz (43% of design frequency) as compared to 3 GHz (27%) with the conventional hybrid. Over the bandwidth, the reflection loss and isolation are below -20 dB. The broader bandwidth is, however, at the expense of a slightly deteriorated performance at 11 GHz.

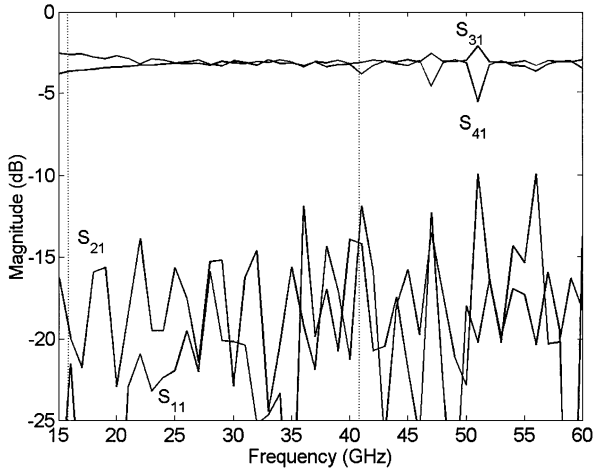

Fig. 13. Simulated frequency response (magnitude) of a stripline FCL section for input at port 1.

V. Broad-Band Stripline FCL Circulator

As mentioned earlier, the design procedure described in [4] is not applicable to a stripline FCL because $\beta_{\rm even} = \beta_{\rm odd}$ at all frequencies. For a stripline FCL with the following parameters: $\varepsilon_f = 12$ (substrate), $\varepsilon_d = 12$ (superstrate), thickness $h_f = h_d = 0.1$ mm, $q = 0.045$ mm, $S = 0.09$ mm, and magnetization $M_s = 239$ kA/m, Xie and Davis [6] found that the predicted PTF and PIF exhibit little variation over the frequency range of 10–50 GHz, but that the onset of a third mode could occur at 41 GHz. Defining the bandwidth as the frequency range where the PIF is below 0.1 (-10 dB) and using 41 GHz as the upper frequency, a center frequency of 26 GHz was selected [6]. However, it should be noted that the bandwidth in [6] is defined including variable optimum FCL lengths, but the predicted optimum length L varied only from 30 to 33 mm over the frequency range of 20–50 GHz. When the structure was simulated using Ansoft HFSS, the optimum length was found to be 28 mm rather than 32 mm. With $L = 28$ mm, it can be seen from the simulated performance in Fig. 13 that the insertion loss S_{31} and S_{41} are approximately -3 dB over a wide frequency range. Spikes occur at frequencies above 41 GHz and these could be due to the higher order mode observed in [6]. Redefining the bandwidth as the frequency range where insertion loss is -3 ± 0.5 dB up to 41 GHz, the bandwidth is from 16 to 41 GHz, i.e., 88% of the center frequency of 28.5 GHz. Over this bandwidth, reflection loss S_{11} and isolation S_{21} are generally below -15 dB. We observe from Fig. 14 that the phase differences at ports 3 and 4 are almost constant at approximately 12° over the defined frequency range, except for a large difference near 33 GHz. The phase differences appear to be less sensitive to frequency than in the microstrip structure. We also observe that the two large positive spikes in the phase behavior occur at the same frequencies as the spikes in the insertion loss

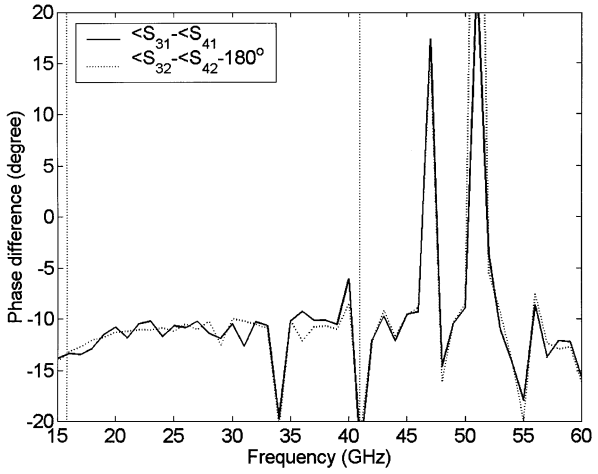

Fig. 14. Predicted frequency response of $\angle S_{31} - \angle S_{41}$ (solid line) and $\angle S_{32} - \angle S_{42} - 180^\circ$ (dotted line) of the FCL section.

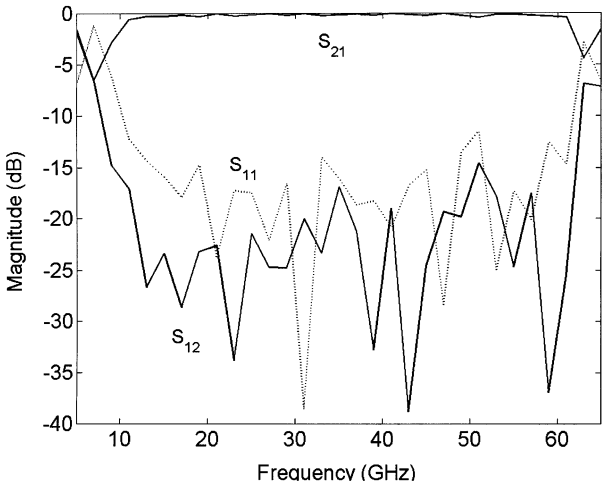

Fig. 15. Predicted frequency response (magnitude) of the three-port stripline FCL circulator.

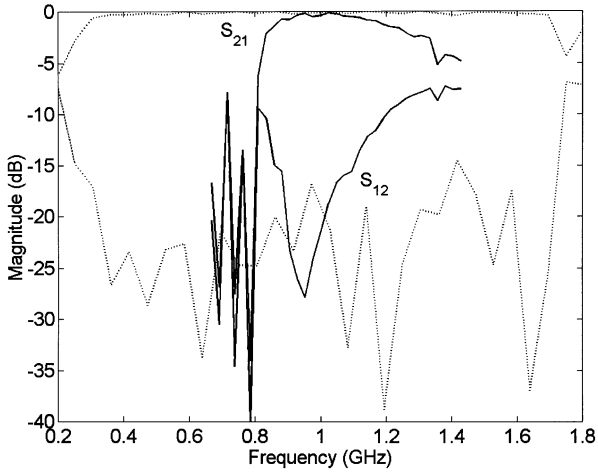

Fig. 16. Comparison between four-port microstrip FCL circulator (solid lines) and three-port stripline FCL circulator (dotted lines), where frequencies are normalized to their respective center frequency.

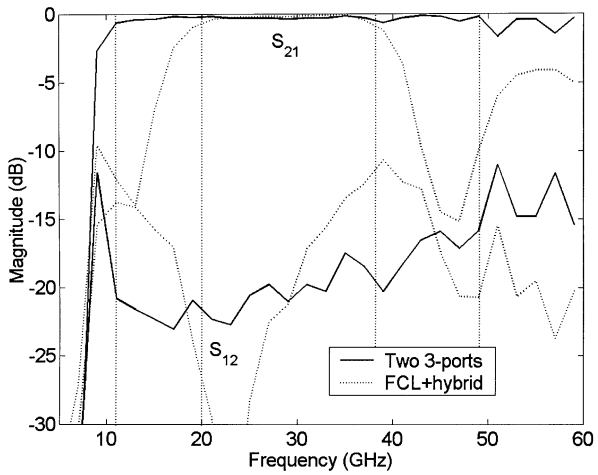

Fig. 17. Comparison of predicted performance (magnitude) between four-port circulators that are made up from: (a) two three-port circulators and (b) an FCL cascaded with a hybrid coupler.

in Fig. 13, whereas the negative spike at 33 GHz in Fig. 14 is not associated with a spike in Fig. 13.

When this broad-band FCL structure is cascaded with a T-junction to form a three-port circulator, its predicted lossless performance using HFSS is as shown in Fig. 15, where the insertion loss S_{21} is less than 0.5 dB from 11 to 61 GHz, while the reflection loss S_{11} and isolation S_{21} are mostly below -15 dB. Also, the spikes at frequencies above 41 GHz, observed in Fig. 13, have vanished and this may be due to the summation in the T-junction of the complimentary spikes observed in S_{31} (upward spikes) and S_{41} (downward spikes). For direct comparison, the insertion S_{21} and isolation S_{12} of the four-port microstrip FCL circulator (from Section III) and the three-port stripline FCL circulator (this section) are plotted in the same graph, as shown in Fig. 16, where frequency of the devices have been normalized to their respective center frequency of 10.5 and 36 GHz. The bandwidth for the latter is clearly much wider than that of the former.

When the same stripline FCL structure is cascaded with a broad-band hybrid coupler designed at 28.5 GHz, the predicted bandwidth of the overall structure is from 20 to 38 GHz, i.e., over 60% of design frequency. This is a significant improvement over the four-port microstrip FCL circulator, which has a 16% bandwidth, and it clearly shows that the limitations due to the microstrip FCL section can be reduced by replacing it with a stripline FCL. In this case, the limitation of the circulator lies in the hybrid coupler. To gain a much broader bandwidth for a four-port circulator, two three-port stripline FCL circulators can be cascaded with each other and, it can be seen from Fig. 17, that the simulated bandwidth is from 11 to 49 GHz, i.e., over 130% bandwidth. Besides being broad-band, the advantage of the four-port circulator made from two three-port circulators is that no air bridge is required due to the absence of the hybrid coupler. However, a disadvantage of such a device might be its relatively greater length and higher conductor loss.

VI. Positioning of Ferrites

With reference to Fig. 1, the effect of ferrite position in either regions I or II on the performance of the circulator has been investigated. For a stripline structure where $d_1 = d_2$, the optimal length of FCL section is unaffected when the ferrite material

TABLE I
EFFECT OF FERRITE POSITIONING TO THE FCL LENGTHS AND OPERATING FREQUENCY

Structure	Microstrip, thin ferrite on top	Microstrip, thick ferrite on top	Microstrip, ferrite on substrate
Details in text	MFCL1	MFCL2	MFCL3
FCL length, L (mm)	62.0	34.5	44.6
Operating freq, f_o (GHz)	7.4	5	4

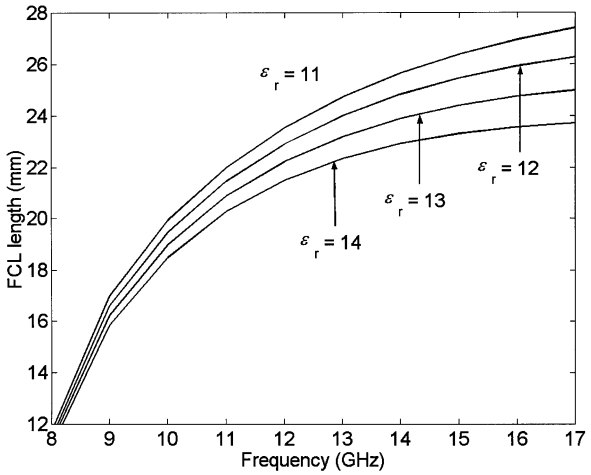

Fig. 18. Effect of ε_f to the optimal length of FCL section.

and the dielectric are exchanged between the two regions, but the direction of circulation is reversed. The effect of ferrite positioning in the microstrip FCL is more complicated as the length of FCL, the operating frequency and the PTFs are affected. Here, we consider three different structures (MFCL1–MFCL3) in which all of them have the following common parameters (all dimensions in millimeters): $q = 0.75$; $b = d_1 + d_2 = 8$, $S = 0.75$, $a = 16$, $\varepsilon_d = 10.2$, $\varepsilon_d = 11.7$, and $M_s = 111$ kA/m ($4\pi M_s = 1400$ G). The three structures are as described below and the computed FCL lengths and operating frequencies are given in Table I.

MFCL1 Microstrip with a thin ferrite on top—this is a three-layer structure with air (h_a 4.976 mm) on the top followed by a thin ferrite material $h_f = 1.5$ mm and then a dielectric of $h_d = 1.524$ mm. This structure has been reported in [7].

MFCL2 Microstrip with a thick ferrite of top, where $d_1 = 6.426$ mm (ferrite) and $d_2 = 1.524$ mm.

MFCL3 Microstrip with a ferrite as a substrate, where $d_1 = 6.5$ mm (air) and $d_2 = 1.5$ mm.

Fields are more concentrated in the substrate of a microstrip line and, hence, the coupling coefficient will be greater if a ferrite is used as a substrate. As a result, the length of MFCL3 is shorter than MFCL1. Also, a thick ferrite on top of the microstrip requires a shorter length than a thin ferrite, i.e., MFCL2 is shorter than MFCL1, because the coupling coefficient is stronger as well due to a larger cross-sectional area of the ferrite. The operating frequency varies for different ferrite positioning due to the dependence of the propagation constants on the effective dielectric of the microstrip. We also observe that, consistent with [6], the maximum PTF is lower for a microstrip with a ferrite as a substrate compared to that of the other two structures. The structure with a ferrite on top is easier to fabricate because the ferrite can be placed on top after the circuit has been fabricated. However, a disadvantage is that the power reflection factor (PRF) will increase due to a mismatch at the isotropic–ferrite interface where the FCL is normally fed by microstrips. The effect of permittivity of the ferrite has been investigated in the case of a thick ferrite on top using the following parameters (all dimension in millimeters): $d_1 = 1.5$, $d_2 = 0.2$, $q = 0.16$, $S = 0.2$, $\varepsilon_r = 10.2$, and $M_s = 239$ kA/m. We see from Fig. 18 that the optimal length of the FCL increases as ε_f decreases, and this is due to higher field concentration in the medium with a higher dielectric constant.

VII. CONCLUSION

Measurements of a four-port microstrip FCL circulator, which includes a rectangular hybrid coupler, have demonstrated a differential isolation greater than 10 dB over a frequency range of 10.4–11.4 GHz. Further work in both the modeling and measurement of FCL structures is required to produce closer agreement between the two and to address some of the problems that have been identified. For example, there is a need for a reliable model to optimize all parameters to obtain the desired amplitude and phase characteristics. Also, further research on loss mechanisms is required because measured insertion losses are higher than can be explained simply in terms of conductor and dielectric losses. However, in principle, very broad bandwidths appear to be possible. Simulation of a lossless three-port stripline FCL circulator has indicated a broad operating bandwidth of at least 10–40 GHz with a differential isolation of greater than 10 dB, an insertion loss of less than 0.5 dB, and with an external bias field of less than 4 kA/m. It may be possible to realize similar structures using high-T_c superconducting circuits and, if so, FCLs would have an advantage that the bias field is parallel with the conductors rather than perpendicular to them.

ACKNOWLEDGMENT

The authors would like to thank N. Priestley, Marconi Applied Technologies, Lincoln, U.K., B. Climer, Marconi Applied Technologies, and K. Newsome, Marconi Applied Technologies, for their assistance with the fabrication and measurement of the four-port microstrip circulator.

REFERENCES

[1] L. E. Davis and D. Sillars, "Millimetric nonreciprocal coupled-slot finline components," *IEEE Trans. Microwave Theory Tech.*, vol. MTT-34, pp. 804–808, July 1986.

[2] J. Mazur and M. Mrozowski, "On the mode coupling in longitudinally magnetized waveguiding structures," *IEEE Trans. Microwave Theory Tech.*, vol. MTT-37, pp. 159–164, Jan. 1989.

[3] J. Mazur, "Millimeter-wave three-port finline circulator using distributed coupling effect," *IEEE Trans. Microwave Theory Tech.*, vol. 41, pp. 1067–1070, June–July 1993.

[4] C. S. Teoh and L. E. Davis, "Normal-mode analysis of ferrite-coupled lines using microstrips or slotlines," *IEEE Trans. Microwave Theory Tech.*, vol. 43, pp. 2991–2998, Jan. 1995.

[5] K. Xie and L. E. Davis, "Nonreciprocity and the optimum operation of ferrite coupled lines," *IEEE Trans. Microwave Theory Tech.*, vol. 48, pp. 562–573, Apr. 2000.
[6] ——, "Performance of axially-magnetized ferrite coupled lines," *Radio Sci.*, vol. 36, no. 6, pp. 1353–1361, Nov.–Dec. 2001.
[7] C. S. Teoh and L. E. Davis, "Design and measurement of microstrip ferrite coupled lines," *Int. J. RF Microwave Computer-Aided Eng.*, vol. 11, no. 3, pp. 121–130, May 2001.
[8] C. K. Queck *et al.*, "Performance of stripline-type FCL circulators," *Int. J. RF Microwave Computer-Aided Eng.*, submitted for publication.
[9] C. K. Queck and L. E. Davis, "Bandwidth and losses of 4-port ferrite coupled line circulator," in *IEEE MTT-S Int. Microwave Symp. Dig.*, vol. 3, Seattle, WA, June 2–7, 2002, pp. 1475–1478.
[10] D. I. Kim, "Broad-band design of improved hybrid-ring 3-dB directional couplers," *IEEE Trans. Microwave Theory Tech.*, vol. 30, pp. 2040–2046, Nov. 1994.
[11] C. K. Queck and L. E. Davis, "Broadband hybrid microstrip couplers—Amplitude and phase," *Microwave Opt. Technol. Lett.*, vol. 32, no. 4, pp. 254–259, Feb. 2002.
[12] T. S. Horng, "A rigorous study of microstrip crossovers and their possible improvements," *IEEE Trans. Microwave Theory Tech.*, vol. 42, pp. 1802–1806, Sept. 1994.
[13] C. K. Queck and L. E. Davis, "Improved design of microstrip air bridges," *Int. J. RF Microwave Computer-Aided Eng.*, submitted for publication.
[14] P. A. Rizzi, *Microwave Engineering Passive Circuits*. Englewood Cliffs, NJ: Prentice-Hall, 1998.
[15] R. A. Pucel *et al.*, "Losses in microstrip," *IEEE Trans. Microwave Theory Tech.*, vol. MTT-16, pp. 342–350, Nov. 1968.
[16] H. A. Wheeler, "Transmission-line properties of parallel strips separated by a dielectric sheet," *IEEE Trans. Microwave Theory Tech.*, vol. MTT-13, pp. 172–185, Mar. 1965.
[17] K. C. Gupta *et al.*, *Microstrip Lines and Slotlines*, 2nd ed. Norwood, MA: Artech House, 1996.

Cham Kiong Queck (S'00) was born in Melaka, Malaysia, on March 28, 1976. He received the B.Eng. degree (with First Class honors) in electrical and electronic engineering from the University of Manchester Institute of Science and Technology (UMIST), Manchester, U.K., in 1999, and is currently working toward the Ph.D. degree in microwave engineering at UMIST.

His research interests are nonreciprocal microwave devices using ferrite material.

Mr. Queck is a student member of the Institution of Electrical Engineers (IEE), U.K. He was the recipient of a Malaysian Government scholarship for undergraduate studies.

Lionel E. Davis (SM'64–LF'95) received the B.Sc. (Eng.) degree from the University of Nottingham, Nottingham, U.K., and the Ph.D. and D.Sc. (Eng.) degrees from University College London, London, U.K.

From 1959 to 1964, he was with Mullard Research Laboratories, Redhill, U.K. From 1964 to 1972, he was a faculty member with the Electrical Engineering Department, Rice University, Houston, TX. From 1972 to 1987, he was with Paisley College, Paisley, Scotland, where he was Professor and Head of the Department of Electrical and Electronic Engineering. In 1987, he joined the Department of Electrical Engineering and Electronics, University of Manchester Institute of Science and Technology (UMIST), Manchester, U.K., where he is currently Professor of communication engineering and Head of the Microwave Engineering Group. He has been a Visiting Professor with the University College London and the University of California at San Diego, and has been a consultant for several companies. He has carried out research on passive components, high-T_c superconductors, dielectric-resonator antennas, chiral materials, and liquid crystal films. His current research interests are in gyrotropic media and nonreciprocal components for microwave, millimeter-wave, and optical wavelengths.

Dr. Davis is a Fellow of the Institution of Electrical Engineers (IEE), U.K., and of the Institute of Physics. He is a member of the IEEE Microwave Theory and Techniques Society (IEEE MTT-S) International Microwave Symposium (IMS) Technical Programme Committee, and co-chairman of the IEEE MTT-S Committee on Microwave Ferrites. Until recently, he was a member of the Administrative Committee of the UKRI MTT/AP/ED/LEOS chapter, and he initiated the Houston chapter of the IEEE MTT-S. He served on the Council, the Microwave Theory and Devices Committee, and the Accreditation Committee of the IEE and is member of the Peer Review College of the U.K. Engineering and Physical Sciences Research Council (EPSRC).